Thermochimica Acta, 164 (1990) 177–189
Elsevier Science Publishers B.V., Amsterdam

THERMAL, ELECTRICAL AND STRUCTURAL PROPERTIES OF CHLORO COMPLEXES OF COBALT, NICKEL, COPPER AND ZINC WITH 6,7-DIMETHYL-2,3-DI(2-PYRIDYL)QUINOXALINE

J.R. ALLAN and A.D. PATON

Department of Applied Chemical Sciences, Napier Polytechnic, Edinburgh (Gt. Britain)

K. TURVEY

Department of Physics, Napier Polytechnic, Edinburgh (Gt. Britain)

(Received 27 November 1989)

ABSTRACT

Some new compounds of 6,7-dimethyl-2,3-di(2-pyridyl)quinoxaline with cobalt(II), nickel(II), copper(II) and zinc(II) have been prepared in toluene. The cobalt and zinc compounds have tetrahedral structures while the nickel and copper complexes have octahedral structures. The thermal behaviour of these compounds has been studied by thermogravimetry and differential thermal analysis. Each compound is highly stable and decomposes, without formation of any intermediate compounds, to the metal oxide. The room temperature conductivities of the prepared compounds are all in the range 3.4×10^{-8} Ω^{-1} m^{-1} to 2.2×10^{-7} Ω^{-1} m^{-1}. Evidence is advanced from current–voltage data and, more especially, from attenuated total reflectance spectra taken during application of an electric field, that the compounds undergo significant field-induced distortion that remains after removal of the field.

INTRODUCTION

Previously reported studies of transition metal complexes with substituted pyrazines include the investigation of their electrical conductivity [1–6], structure [1,3,4,6] and thermal stability [2,5,6]. The largest observed electrical conductivities at room temperature were for compounds containing quinoxaline molecules [5]. As a large electrical conductivity is a prerequisite for most device applications, the high conductivity for the quinoxaline compounds has led us to consider transition metal complexes with other quinoxaline derivatives. The present paper reports investigations of the thermal stability, structure and electrical properties for compounds formed by complexing cobalt, nickel, copper and zinc with the substituted quinoxaline 6,7-dimethyl-2,3-di(2-pyridyl)quinoxaline. Thermogravimetry and differential thermal analysis were used to study thermal stability, spectroscopic

0040-6031/90/$03.50

and magnetic measurements were used to infer structure, and d.c. electrical measurements were used to obtain the electrical conductivity and the activation energy for carriers. From a literature search, there appears to be no record of previous preparations of these compounds.

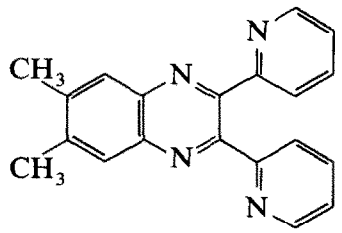

6,7-Dimethyl-2,3-di(2-pyridyl)quinoxaline ($C_{20}H_{16}N_4$).

EXPERIMENTAL

Preparation of complexes

2.5 mmol of 6,7-dimethyl-2,3-di(2-pyridyl)quinoxaline was dissolved in 80 cm^3 of a 1 : 1 mixture of toluene and ethanol. The mixture was refluxed for 30 min. A solution of 2.5 mmol of the metal(II) halide in 10 cm^3 of ethanol was added to the refluxing mixture. Refluxing of the solution was continued for a further 2 h. The precipitated product was isolated by filtration and washed with a minimum of ethanol and then dried in an oven at 40 °C.

Analytical, magnetic, spectral and thermal measurements

The analysis of the metal ion was determined using a Perkin–Elmer 373 atomic absorption spectrophotometer and carbon, hydrogen and nitrogen analyses were obtained using a Carlo Erba elemental analyser. Magnetic moments of the compounds were measured by the Gouy method using $Hg[Co(SCN)_4]$ as calibrant with a correction involving Pascal's constants [7] applied for diamagnetism. Electronic spectra were obtained on a Beckmann Acta MIV spectrophotometer as solid diffuse reflectance spectra. Infrared spectra, using KBr discs in the range 4000–600 cm^{-1} and polyethylene discs in the range 600–200 cm^{-1} were recorded by a Perkin–Elmer infrared spectrophotometer model 598. The thermal analysis measurements were performed using a Stanton Redcroft model STA 781 thermobalance. Thermogravimetry (TG) and differential thermal analysis (DTA) traces were obtained at a heating rate of 6 °C min^{-1} in static air. In all cases the 20–800 °C temperature range was studied.

Electrical and electro-reflectance measurements

For the electrical measurements the complexes, which were prepared in powder form, were compressed into discs of diameter 13 mm and thicknesses in the range 0.92–1.43 mm using a hydraulic press which applied a force of 100 kN. A conducting silver paint electrode of diameter 4.9 mm was applied concentrically on the flat face of each disc. To ensure a sharply defined edge to these electrodes a mask was used during painting. The room temperature conductivity was obtained by measuring the current passed through each disc as a function of the applied voltage using a d.c. circuit in which the current measurement was by a Keithley 610C electrometer connected so as to register only the disc current. The disc was mounted with the lower electrode on a copper base and a spring-loaded pad made contact to the upper electrode. The disc thickness, which is needed to compute the conductivity from the electrical measurements, was obtained using a micrometer.

Measurements were taken of the temperature dependence of the conductivity by placing each disc in an oven and monitoring the current passed during constant application of 10 V across the electrodes whilst the disc was heated to no more than 352 K. Cooling was allowed to occur and additional measurements obtained. The disc temperature was found from the EMF of a previously calibrated copper–constantan thermocouple (44 SWG wires) with its hot junction in contact with the disc and its cold junction in melting ice.

Attenuated total reflectance (ATR) IR spectroscopy was used to investigate possible structural changes in the molecules induced by an electric field.

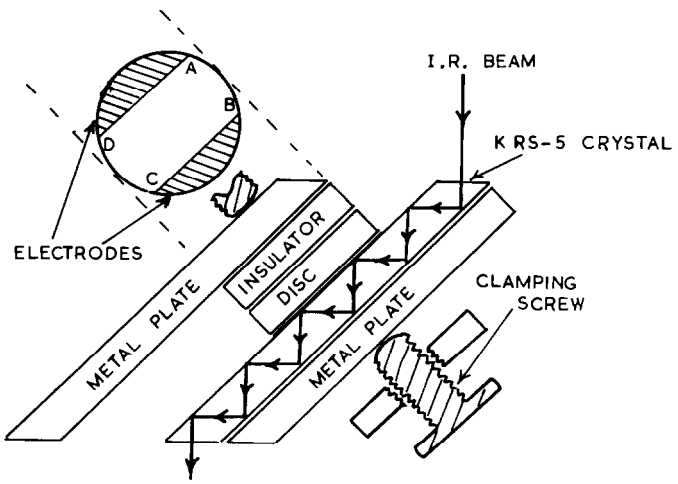

Fig. 1. Method used to obtain ATR spectra at room temperature. The electrode arrangement on a disc of $Ni(C_{20}H_{16}N_4)Cl_2$ is as shown in the plan view. The electrodes continue around the disc edge to a similar arrangement on the reverse side. The region ABCD of the disc is in contact with the KRS-5 crystal.

For this technique, which was used only for the nickel compound, a new disc of compressed powder was prepared as previously described. Silver conductive paint electrodes were applied as shown in plan view in Fig. 1. The electrode geometry on the reverse face of the disc is identical and contact between the electrode sections on the two faces is by conductive paint along the rim. The region ABCD (Fig. 1) on one side of the disc was placed in contact with a KRS-5 (mixed thallous bromide/iodide) crystal used as an ATR accessory to a Pye–Unicam SP3-300 IR double-beam spectrophotometer. Computerised data handling techniques were used in which multiple scans (10 were used) of the spectrum were taken to obtain a good signal to noise ratio. Spectra were obtained over the range 3200–600 cm^{-1} under the following conditions: A, no voltage applied across the electrodes; B, during application of 25 V across the electrodes; and C, during application of 25 V across the electrodes but with reversed polarity compared with B. Additional spectra were also obtained after runs B and C following shorting of the electrodes to remove any residual polarisation.

RESULTS AND DISCUSSION

Analytical

Table 1 shows the analytical results for the complexes; in each case there is good agreement with the given molecular formula.

Electronic spectra

The wavenumbers of the d–d bands in the electronic spectra of the cobalt, nickel and copper complexes are given in Table 2. The positions of these bands indicates that the metal ion environment is octahedral in the nickel and copper complexes [8,9] whilst it is tetrahedral in the cobalt complex [10]. The *Dq* values in Table 2 for the cobalt and nickel complexes are consistent with the suggested stereochemistry [11].

Magnetic moments

The magnetic moments for the cobalt and nickel compounds are in the ranges 4.2–4.8 B.M. and 2.8–3.4. B.M. respectively (see Table 1). This supports the earlier suggestion that the cobalt and nickel atoms are in tetrahedral and octahedral environments respectively [8,10]. The magnetic moment for the copper compound exceeds the spin-only value of 1.73 B.M. by 6.4%; this is attributed to an orbital contribution.

TABLE 1

Analyses and magnetic moments of compounds

Compound	Colour	Theory (%)				Found (%)				μ (B.M.)
		Metal	Carbon	Nitrogen	Hydrogen	Metal	Carbon	Nitrogen	Hydrogen	
$Co(C_{20}H_{16}N_4)Cl_2$	Dark green	13.32	54.32	12.67	3.65	13.12	54.30	12.36	3.41	4.30
$Ni(C_{20}H_{16}N_4)Cl_2$	Yellow-brown	13.28	54.35	12.68	3.65	13.08	54.18	12.62	3.61	3.05
$Cu(C_{20}H_{16}N_4)Cl_2$	Brown	14.22	53.76	12.54	3.61	14.12	53.50	12.29	3.38	1.84
$Zn(C_{20}H_{16}N_4)Cl_2$	White	14.57	53.54	12.49	3.60	14.43	53.60	12.50	3.46	–

TABLE 2

Electronic spectra

Compound	Peak position (cm^{-1})	d–d transition	Dq [a] (cm^{-1})	B [b] (cm^{-1})	β [c] (cm^{-1})
$Co(C_{20}H_{16}N_4)Cl_2$	9615	$^4A_2(F) \rightarrow {}^4T_1(F)$	517	717	0.74
	16666	$^4A_2(F) \rightarrow {}^4T_1(P)$			
$Ni(C_{20}H_{16}N_4)Cl_2$	8826	$^3A_{2g}(F) \rightarrow {}^3T_{2g}(F)$	882	827	0.79
	14797	$^3A_{2g}(F) \rightarrow {}^3T_{1g}(F)$			
	24091	$^3A_{2g}(F) \rightarrow {}^3T_{1g}(P)$			
$Cu(C_{20}H_{16}N_4)Cl_2$	10752	$^2E_g(D) \rightarrow {}^2T_{2g}(D)$			

[a] Dq is the ligand field strength.
[b] B is the Racah parameter.
[c] β is the nephelauxetic ratio.

IR spectra

The wavenumbers of the IR absorption bands, as well as their descriptions and assignments, are given in Table 3. Although the table does not give full details, the infrared spectrum of 6,7-dimethyl-2,3-di(2-pyridyl)quinoxaline is similar to that of its complexes in the 2000–600 cm^{-1} region except for the bands due to the ring vibrations of the aromatic ring which are at higher frequencies in the complexes than in the free ligand. This suggests that in each complex the nitrogen atom in the aromatic ring is coordinated to a metal ion [8,9]. Metal–halogen vibrations are observed for the complexes and are also reported in Table 3. The assignments made for these ν(M–X) vibrations are consistent with the metal ions having a tetrahedral environment in the cobalt and zinc complexes but an octahedral environment in the nickel and copper complexes [8,9,11,12].

Proposed stereochemistry

No single crystals of the compounds were isolated from solution. Thus, without X-ray analysis, no definite structure can be described. However, the

TABLE 3

IR spectra (4000–200 cm^{-1})

Compound	Ring vibrations [a] (cm^{-1})				ν(M–X) [b] (cm^{-1})	
$C_{20}H_{16}N_4$	1585(s)	1566(s)	1470(s)	1350(s)		
$Co(C_{20}H_{16}N_4)Cl_2$	1601(s)	1582(s)	1475(s)	1356(s)	315(m)	300(m)
$Ni(C_{20}H_{16}N_4)Cl_2$	1596(s)			1366(s)	254(m)	
$Cu(C_{20}H_{16}N_4)Cl_2$	1598(s)	1581(s)		1356(s)	276(m)	
$Zn(C_{20}H_{16}N_4)Cl_2$	1603(s)		1480(s)	1354(s)	338(s)	308(s)

[a] s, Strong; m, medium.
[b] Metal–halogen vibration frequencies.

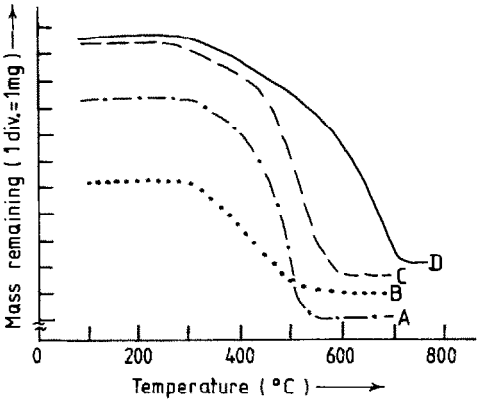

Fig. 2. Thermogravimetric curves for the $M(C_{20}H_{16}N_4)Cl_2$ compounds: A, M = Co, initial mass = 9.50 mg; B, M = Ni, initial mass = 4.75 mg; C, M = Cu, initial mass = 9.80 mg; and D, M = Zn, initial mass = 9.84 mg. The curves are shifted by different amounts in the vertical direction.

spectroscopic and magnetic data enable possible structures to be predicted. The ligand 6,7-dimethyl-2,3-di(2-pyridyl)quinoxaline has four coordinating nitrogen atoms and the stereochemistry dictates that the nitrogen atoms coordinate in pairs with the metal ions in nickel and copper complexes, thereby linking together adjacent ligand molecules. We thus postulate a planar arrangement for every four nitrogen atoms. The six-coordinate environment for each nickel or copper ion is completed by a bonding chlorine atom on either side of the plane. In the cobalt and zinc complexes the metal ion is bonded to two chlorine atoms, a nitrogen atom of a pyridine ring and a nitrogen atom of a pyrazine ring to give a tetrahedral structure.

Thermal analysis

The TG curves for the chloro complexes of cobalt, nickel, copper and zinc with 6,7-dimethyl-2,3-di(2-pyridyl)quinoxaline are shown in Fig. 2. The compounds undergo decomposition with loss of organic ligand and the

TABLE 4

Decomposition processes of the metal complexes

Complex	Temperature range (°C)	Thermal nature of transformation [a]	Residue weights (%)	
			Calc.	Found
$Co(C_{20}H_{16}N_4)Cl_2$	290–548	Exo	18.14	17.36
$Ni(C_{20}H_{16}N_4)Cl_2$	305–618	Exo	16.90	17.89
$Cu(C_{20}H_{16}N_4)Cl_2$	248–620	Exo	17.99	16.32
$Zn(C_{20}H_{16}N_4)Cl_2$	310–724	Exo	18.40	18.29

[a] Exo, Exothermic (obtained from DTA curve).

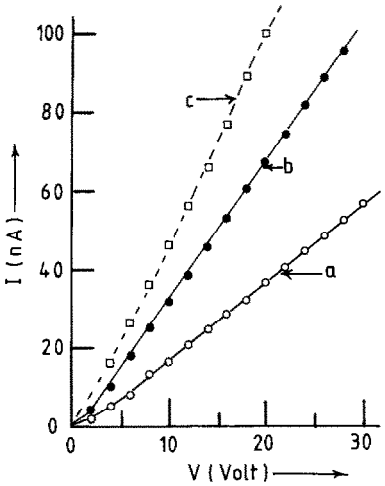

Fig. 3. Plots of current I versus voltage V for a disc of $Ni(C_{20}H_{16}N_4)Cl_2$ at room temperature. Curve a, initial polarity of applied voltage. Points plotted show mean currents for increasing and decreasing voltage. Curve b, polarity of applied voltage reversed after obtaining curve a. The points plotted for the reversed polarity show mean currents for increasing and decreasing voltage. Curve c, polarity of applied voltage returned to that for curve a. The points show currents as the applied voltage is increased. Note that curve c does not reproduce curve a.

formation of the metal oxide. The residue weights, see Table 4, are in good agreement with the values required for the metallic oxides. The order of stability, based on the initial decomposition temperatures of the metal complexes, can be listed as: $Zn(C_{20}H_{16}N_4)Cl_2 > Ni(C_{20}H_{16}N_4)Cl_2 > Co(C_{20}H_{16}N_4Cl_2 > Cu(C_{20}H_{16}N_4)Cl_2$ where $C_{20}H_{16}N_4$ is 6,7-dimethyl-2,3-di-(2-pyridyl)quinoxaline.

Electrical conduction

The room temperature current I versus voltage V characteristics for discs of the nickel and zinc complexes are shown in Figs. 3 and 4 respectively. The curves labelled a, b and c in these figures refer to the first direction of applied polarity, the reversed polarity and a return to the original direction, respectively. Data for plotting the a and b curves were obtained for both increasing and decreasing magnitude of applied voltage. A difference of a few per cent was noted between the currents for these two directions, so slight hysteresis exists, but the plotted points show mean currents. For both compounds, curve b is above curve a, and curve c, which forms a repeat for the same polarity as curve a, does not reproduce curve a.

The cobalt and copper compounds, for which the I versus V curves are not shown, also exhibit larger currents under the second (i.e. reversed) polarity than for the initial polarity but, unlike the nickel and zinc com-

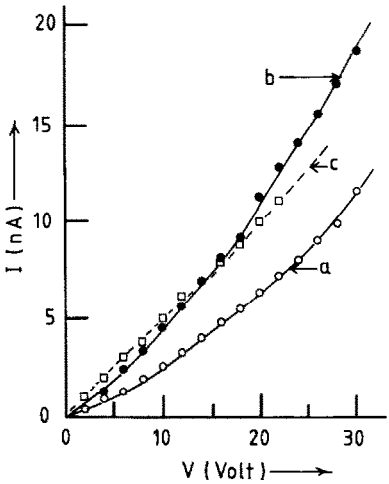

Fig. 4. Plots of current I versus voltage V for a disc of $Zn(C_{20}H_{16}N_4)Cl_2$ at room temperature. Curve a, initial polarity of applied voltage. Points plotted show mean currents for increasing and decreasing voltage. Curve b, polarity of applied voltage reversed after obtaining curve a. The points plotted for the reversed polarity show mean currents for increasing and decreasing voltage. Curve c, polarity of applied voltage returned to that for curve a. The points show currents as the applied voltage is increased. Note that curve c does not reproduce curve a.

plexes, no detectable difference in current is found between increasing or decreasing voltage magnitude, i.e. hysteresis is negligible. The initial polarity was not re-applied for the cobalt and copper compounds.

The summary of the results reported above for the I versus V characteristics at room temperature is that for all four complexes, reversal of the polarity after the original voltage application leads to an increase in conductivity and for the two complexes which were then tested again with restoration of the original polarity, the conductivity is increased compared to the original measurement. These results suggest that an applied electric field distorts the molecules and that much of this distortion remains after removal of the field. A current contribution during the distortion may account for the hysteresis noted in the I–V characteristics of the nickel and zinc compounds.

The room temperature conductivities, as determined for the final polarity used, are given in Table 5. In computing these conductivities it is assumed that the current density vector is normal to the electrodes throughout the disc. The arbitrarily chosen field of 1×10^4 V m^{-1} for the quoted conductivities is in the middle of the range of applied fields. (Because the behaviour is slightly non-ohmic it follows that the conductivity is weakly dependent on the field.) The conductivities are several orders of magnitude lower than the previously reported [5,6] maximal values found for either quinoxaline complexes or methylquinoxaline complexes measured under identical conditions. If it is assumed that all measured conductivities reflect intrinsic as opposed

TABLE 5

Electrical properties of the compounds

Compound	Conductivity [a] at room temperature (Ω^{-1} m^{-1})	ΔE [b] (eV)		
		Heating	Cooling	Combined heating and cooling
$Co(C_{20}H_{16}N_4)Cl_2$	6.2×10^{-8}	1.28	2.06	1.70
$Ni(C_{20}H_{16}N_4)Cl_2$	2.2×10^{-7}	0.76	1.94	1.40
$Cu(C_{20}H_{16}N_4)Cl_2$	8.6×10^{-8}	1.15	1.54	1.34
$Zn(C_{20}H_{16}N_4)Cl_2$	3.4×10^{-8}	1.14	2.02	1.64

[a] Values refer to a field of 1×10^4 V m^{-1}.

[b] ΔE is the energy in the equation $\sigma = \sigma_0 \exp(-\Delta E/2kT)$.

to impurity-dominated values then it appears that the addition of the pyridyl groups suppresses the conductivity.

Figure 5 shows Arrhenius plots (in the form of graphs of ln σ versus T^{-1}, where σ is the conductivity at absolute temperature T) for the zinc and copper complexes based on conductivity measurements under application of 10 V to the same discs as were used for the room temperature measurements. Similar plots based on corresponding measurements for the nickel

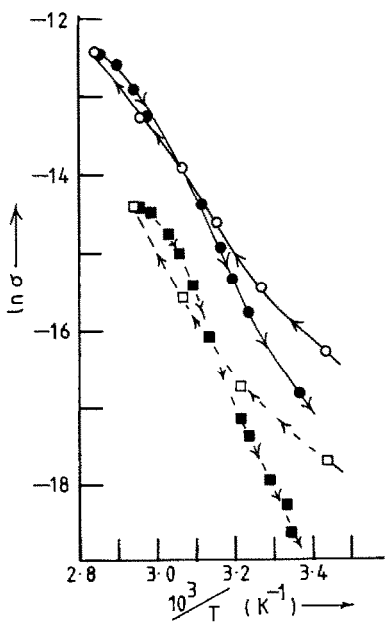

Fig. 5. Plots of ln σ versus $10^3\times T^{-1}$ (where σ is the conductivity in units of Ω^{-1} m^{-1} at absolute temperature T) for discs of: $Cu(C_{20}H_{16}N_4)Cl_2$ (○———○, increasing T; ●———●, decreasing T) and $Zn(C_{20}H_{16}N_4)Cl_2$ (□— — —□, increasing T; ■— — —■, decreasing T).

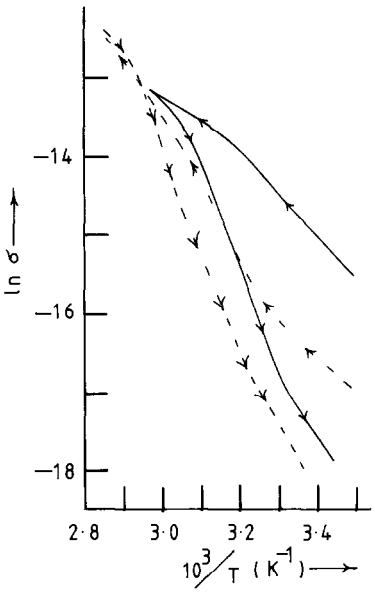

Fig. 6. Plots of ln σ versus $10^3 \times T^{-1}$ (where σ is the conductivity in units of Ω^{-1} m^{-1} at absolute temperature T) for discs of: $Ni(C_{20}H_{16}N_4)Cl_2$, (———); and $Co(C_{20}H_{16}N_4)Cl_2$, (— — —).

and cobalt complexes are shown in Fig. 6. The activation energy ΔE appearing in the equation $\sigma = \sigma_0 \exp(-\Delta E/2kT)$, in which σ_0 is a constant, is listed for each compound in Table 5 and is found from the gradient of the least-squares-fitted line through the points of the Arrhenius plot. However, as seen from Figs. 5 and 6, the linearity is not high and the cooling data do not agree with that for heating. Thermal decomposition is not the cause of the poor agreement between the sections of the curves in Figs. 5 and 6 that relate to heating and cooling because the maximum temperature reached (352 K) is far below that already found for the onset of decomposition (see Table 4). Consideration was given to the possibility that although heating to 352 K produces no decomposition, the bonding may be altered through tangling or locked-in twisting. However, this hypothesis of a purely thermally-induced structural change is rejected because room temperature infrared absorption spectra taken over the wavenumber range 1400–600 cm^{-1} for a fresh specimen of the nickel compound (which is the compound exhibiting the greatest difference between conductivities measured under heating and cooling conditions) are identical before and after heating to 352 K. In collecting the data for Figs. 5 and 6, it is possible that the oxidation state of traces of donor or acceptor impurities was permanently altered; this would be manifested as a large change in electrical properties with negligible associated spectral change. Arrhenius plots of similar shape to those in Figs. 5 and 6 were found in a previous study [6] of other quinoxaline-based complexes.

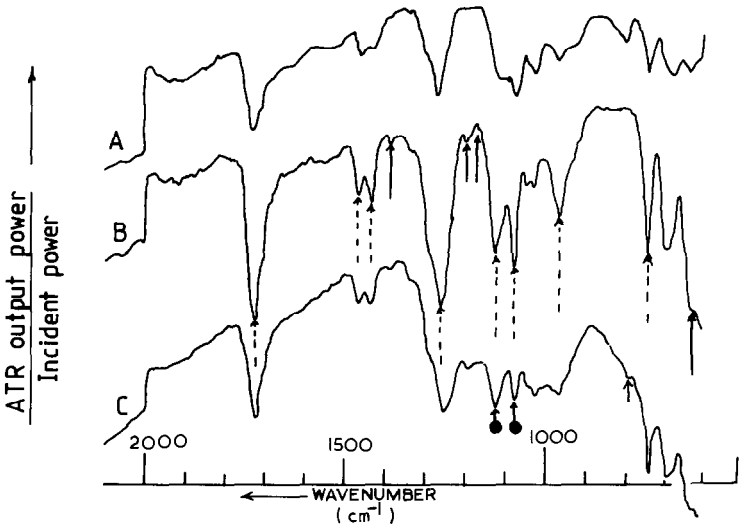

Fig. 7. Spectra obtained using the ATR technique shown in Fig. 1: A, no voltage applied across electrodes; B, 25 V applied across electrodes; and C, 25 V (in the reverse polarity to that of curve B) applied across the electrodes. →, New absorption lines not observed in preceding spectrum; --→, absorption lines that are more prominent than in preceding spectrum; and ● →, two absorption lines in curve C that have interchanged in magnitude relative to that in curve B.

The ATR spectra, Fig. 7, show that application of an electric field to the nickel compound whilst at room temperature produces additional absorption lines and enhances the absorption corresponding to certain other lines. Modification to the absorption spectrum resulting from application of an electric field was not investigated for the other compounds. The choice of the nickel compound is because it exhibits the largest hysteresis in its room temperature I–V characteristics. Curve C of Fig. 7 which refers to reversed voltage polarity after obtaining curve B, also shows that the relative absorptions for two neighbouring lines near a wavenumber of 1100 cm^{-1} interchange compared with those in curve B. The ATR spectra therefore confirm that the molecules distort in some way on application of an electric field, as already suggested to explain the hysteresis in the room temperature I–V characteristics. For the 6,7-dimethyl-2,3-di(2-pyridyl)quinoxaline ligand a possible distortion would be due to torsion in the bonds between the pyrazine and pyridine rings, although in the complexes the bonding of the metal ions would impose more rigidity against such torsional displacements. Since the spectral region covered by Fig. 7 is rich in absorption lines due to in-plane and out-of-plane vibrations of both the pyrazine and pyridine rings, it appears that the field-induced distortion is in these rings. Immediately following the collection of the spectral curves B and C in Fig. 7, the electrodes were shorted and additional ATR spectra were taken that are not displayed in the figure. These spectra are identical to B and C respectively,

indicating that the field-induced distortion remains after removal of the field. The magnitude of the applied field during collection of the ATR spectra is weak compared with that during the measurement of the $I-V$ curves (because the applied voltages are similar but the inter-electrode distance is greater for the ATR spectra) yet the spectra clearly reveal field-induced molecular distortion.

REFERENCES

1 J.R. Allan, H.J. Bowley, D.L. Gerrard, A.D. Paton and K. Turvey, J. Coord. Chem., 17 (1988) 255.
2 J.R. Allan, H.J. Bowley, D.L. Gerrard, A.D. Paton and K. Turvey, Thermochim. Acta, 124 (1988) 345.
3 J.R. Allan, H.J. Bowley, D.L. Gerrard, A.D. Paton and K. Turvey, Inorg. Chim. Acta, 132 (1987) 41.
4 J.R. Allan, H.J. Bowley, D.L. Gerrard, A.D. Paton and K. Turvey, Inorg. Chim. Acta, 134 (1987) 259.
5 J.R. Allan, H.J. Bowley, D.L. Gerrard, A.D. Paton and K. Turvey, Thermochim. Acta, 122 (1987) 403.
6 J.R. Allan, D.L. Gerrard, S. Hoey, A.D. Paton and K. Turvey, Thermochim. Acta, 145 (1989) 291.
7 B.N. Figgis and J. Lewis, in J. Lewis and R.G. Wilkins (Eds.), Modern Coordination Chemistry, Interscience, New York, 1960, p. 403.
8 J.R. Allan, N.D. Baird and A.L. Kassyk, J. Therm. Anal., 16 (1979) 79.
9 J.R. Allan, G.M. Baillie and N.D. Baird, J. Coord. Chem., 10 (1979) 171.
10 J.R. Allan and G.M. Baillie, J. Therm. Anal., 14 (1978) 291.
11 A.B.P. Lever, Inorganic Electronic Spectroscopy, Elsevier, London, 1968, pp. 324, 336.
12 J.R. Allan, D.H. Brown, R.H. Nuttall and D.W.A. Sharp, J. Chem. Soc., (1966) 1031.